Strong Carbon Nanotube Fibers by Drawing Inspiration from Polymer Fiber Spinning

Belén Alemán, Víctor Reguero, Bartolomé Mas, and Juan J. Vilatela*

IMDEA Materials Institute, c/Eric Kandel 2, Getafe 28906, Madrid, Spain

ABSTRACT We present a method to spin highly oriented continuous fibers of adjustable carbon nanotube (CNT) type, with mechanical properties in the high-performance range. By lowering the concentration of nanotubes in the gas phase, through either reduction of the precursor feed rate or increase in carrier gas flow rate, the density of entanglements is reduced and the CNT aerogel can thus be drawn (up to 18 draw ratio) and wound at fast rates (>50 m/min). This is achieved without affecting the synthesis process, as demonstrated by Raman spectroscopy, and implies that the parameters controlling composition in terms of CNT diameter and number of layers are decoupled from those fixing CNT orientation. Applying polymer fiber wet-spinning principles then, strong CNT fibers (1 GPa/SG) are produced under dilute conditions and high draw ratios, corresponding to highly aligned fibers (from wide- and small-angle X-ray scattering). This is demonstrated for fibers either made up of predominantly single-wall CNTs (SWCNTs) or predominantly multiwall CNTs (MWCNTs), which surprisingly have very similar tensile properties. Finally, we show that postspin densification has no substantial effect on either alignment or properties (mechanical and electrical). These results demonstrate a route to control CNT assembly and reinforce their potential as a high-performance fiber.

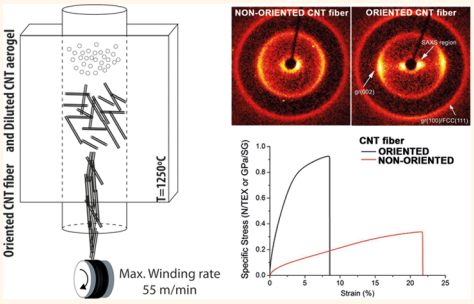

KEYWORDS: CNT fiber · CVD synthesis · fiber orientation · dilution · drawing · polymer · high-performance

One of the most difficult challenges associated with nanomaterials is the exploitation of their exceptional properties on a macroscopic length scale. Their properties at the nanoscale are similar or superior to those of a "single crystal" while extending over macroscopic lengths. In the case of the nanocarbons (CNTs and graphene), for example, experimental measurements put CNT tensile strength and elastic modulus on par with in-plane graphite at around 100 GPa and 1 TPa,[1] respectively, with electron mobility > 100 000 $cm^2/(V\ s)$[2] and thermal conductivity in the 700−3000 W/mK range.[3,4] Yet, producing a macroscopic nanocarbon-based material requires assembling a large number of these building blocks, and the properties of the final material can be strongly dictated by characteristics of the ensemble. Integrating nanocarbons as fillers in polymer matrices results in an intrinsic trade-off between dispersion and volume fraction and is therefore effective only at low volume fractions below about 1 vol %.[5] In contrast, assembling them into macroscopic fibers made up entirely of CNTs can result in materials with mechanical properties in the high-performance range,[6−8] rivaling carbon fiber, for example, with electrical conductivity per unit mass close to that of metals.[9,10] This is the case when the nanocarbon building blocks are aligned parallel to each other and to the fiber axis, in an architecture that efficiently exploits their axial (in-plane) properties. This arrangement is in line with Staudinger's[11] and Carother's[12] models for producing strong fibers from extended highly oriented rigid molecules, proposed nearly a century ago, and which has been the inspiration for a vast library of high-performance polymer fibers made of polyethylene (PE, Dyneema), *p*-phenylene terephthalamide (PPTA, Kevlar), poly(*p*-phenylene-2,6-benzobisoxazole) (PBO, Zylon), *etc.*

CNTs are indeed similar to polymer chains[13] and can behave like rigid conjugated polymers, albeit with a much higher persistence length than for a rigid-rod polymer such as PBO.[14] Furthermore, from either dispersions in polymer solution[15] or lyotropic-nematic liquid crystal phases,[16]

* Address correspondence to juanjose.vilatela@imdea.org.

Received for review April 22, 2015 and accepted June 17, 2015.

Published online June 17, 2015
10.1021/acsnano.5b02408

they can be spun as continuous macroscopic fibers, in a process very similar to polymer fiber wet spinning.

In this work, we demonstrate that the polymer analogy can be extended to CNT fibers produced directly from the gas phase during chemical vapor deposition (CVD). By controlling the dilution of CNTs in the gas phase, it is possible to reduce the number of entanglements in the aerogel, similar to the dilution applied in wet spinning of gel polymer fibers, thus enabling the drawing of the in-forming fiber and alignment of its building blocks. This is achieved for any CNT type from SWCNTs, collapsed to MWCNTs, without affecting the CVD reaction. The orientation of elements results in better packing of CNTs and bundles in the fiber, measured by 2D wide- and small-angle X-ray scattering (WAXS/SAXS), and increases tensile strength and modulus from 0.3 to 1 GPa/SG and 5 to 40 GPa/SG, respectively. These results provide a rational method to produce continuous fibers of specific types of CNTs and tensile properties in the high-performance range.

RESULTS AND DISCUSSION

Assembly Stage in the Direct Spinning Method. The assembly of CNTs into a fiber in the direct spinning method occurs in the gas phase, where the very long CNTs (1 mm) entangle and form an aerogel, which is then drawn through and out of the reactor tube and continuously deposited onto a winder. The action of drawing the aerogel has two effects: it condenses the aerogel into a denser fiber and orients the CNTs preferentially parallel to each other and to the fiber axis. This occurs because as the aerogel is drawn substantially faster (>5 m/min) than the carrier gas velocity (<1 m/min), it is effectively dragged against the gas, similar to a spider web in damping motion,[17] producing frictional shear forces acting on the high-surface CNTs and responsible for their alignment and assembly. Thus, the rate at which the aerogel is drawn is a fundamental parameter controlling the final fiber structure and tensile properties.[6] In the exploration of the parameter space of this process, we have observed that the "dilution" of the aerogel through either a decrease in precursor feed rate or an increase in hydrogen carrier gas flow rate enables much faster fiber drawing rates. This is schematically shown in Figure 1a, representing two different CVD growth conditions, one enabling the orientation of CNT bundles through drawing at fast rates (up to 55 m/min) and the other producing a CNT aerogel that can only be extracted from the reactor but not substantially drawn in the process (up to 8 m/min). Examples of electron micrographs showing the differences in CNT alignment are included in Figure 1b,c.

The maximum winding rate, W_{max}, is a good indicator of how much an aerogel can be drawn during the spinning process and, thus, a good figure of merit of orientability when exploring the spinning parameter space. Figure 2a presents a 3D plot of W_{max} against precursor feed rate and H_2 carrier gas flow. The data included are for three different compositions of the precursor mixture (0.2, 0.8, and 1.5 wt % thiophene) targeting SWCNTs, DWCNTs, and MWCNTs.[18] Irrespective of thiophene (*i.e.*, sulfur) content in the mixture, the data points converge to higher winding rates enabled by low feed rates and/or higher H_2 flow rates. We note that the window of orientable fibers shown here corresponds to conditions under which kilometers of continuous CNT fiber can be spun (see video in the SI), but the intrinsic window in terms of aerogel properties is probably larger once the specific details of the spinning reactor design are factored out. Our data at the lower end of feed rates approach the limit of our liquid injection equipment, whereas the highest hydrogen flow currently limits winding due to practical difficulties in extracting the wide aerogel from the reactor.

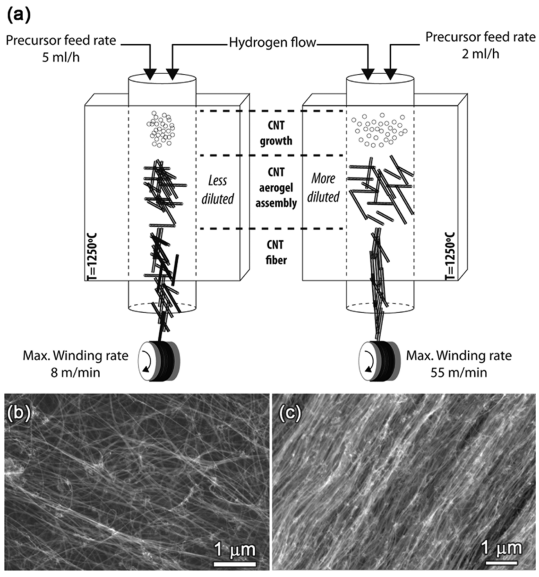

Figure 1. (a) Schematic representation of the direct CNT fiber spinning process showing the effect of aerogel dilution on the orientability of the final fibers. Scanning electron micrographs of (b) nonoriented and (c) oriented CNT fibers.

Sections of the 3D plot at constant hydrogen flow (Figure 2b) and constant feed rate (Figure 2c) show the equivalent role of the two parameters in diluting the system and leading to higher values of W_{max}. Intuitively, when the CNT aerogel is more diluted (the density of CNTs in the gas phase is low), it has a lower density of entanglements and can therefore withstand more drawing, leading to faster winding/spinning rates. In the curves in Figure 2 we have also included an approximate draw ratio for the corresponding winding rate maxima. This is obtained by defining zero draw as the minimum winding rate achievable without accumulation of fiber in the reactor, corresponding to 3 m/min under the synthesis conditions used here.

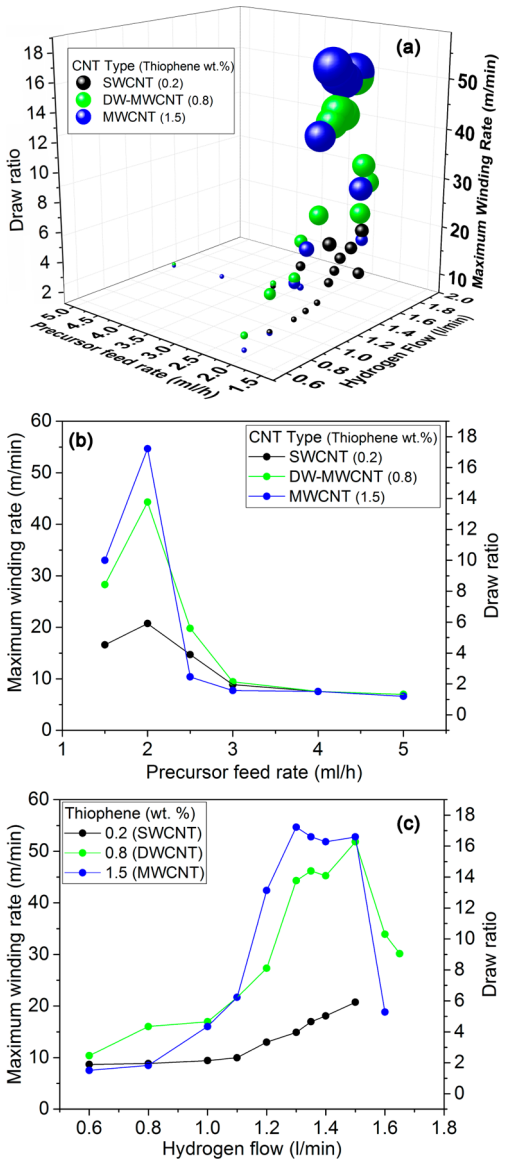

Figure 2. Dependence of the maximum winding rate on precursor feed rate and hydrogen flow, showing that faster rates are obtained in dilute conditions when the concentration of particles (CNTs) in the gas phase is lower and therefore the possibility to draw the aerogel and orient the CNTs is higher. (a) Surface plot of parameter space for different aerogel compositions. Constant hydrogen flow (b) and constant feed rate (c) sections of parameter space showing the equivalent role of these two parameters in diluting the aerogel.

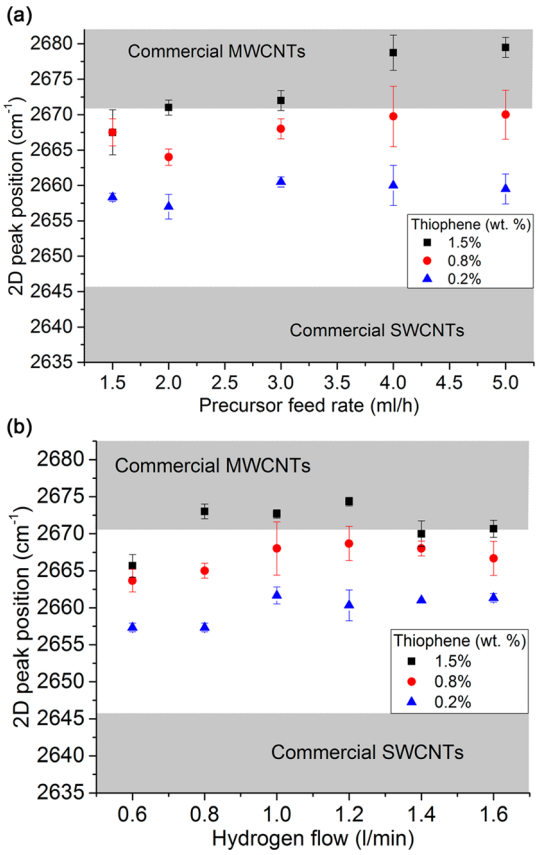

Figure 3. 2D Raman band position dependence on (a) precursor feed rate and (b) hydrogen flow for three types of CNT fibers showing that the CNT fiber composition is not significantly altered when controlling the assembly through dilution.

An important aspect of controlling CNT assembly in the gas phase is to achieve this with minimum effect on the CVD reaction and thus on the composition of the fiber in terms of the type of CNTs. Raman spectroscopy measurements confirm that varying the feed rate and hydrogen flow rates in the ranges in Figure 2 does not produce significant changes in the composition of the fiber (full spectra in S1). Figure 3 shows that the position of the 2D (G′) band, highly sensitive to the number of graphitic layers,[19] remains nearly constant as precursor feed rate (Figure 3a) and hydrogen flow rate (Figure 3b) are varied. Interestingly, increasing the feed rate of precursors does not lead to an increase in CNT diameter through coarsening of catalyst particles. Instead, our results confirm that within the parameters of this work the type of CNT in terms of number of layers is dictated by the precursor mixture, particularly the ratio of S/C,[18] whereas feed rate and hydrogen gas flow, while enabling the catalytic reaction, also have the secondary role of fixing the aerogel constitution and thus the possibility of CNT assembly into the final fiber.

A direct indication of CNT dilution in the gas phase is obtained by visual inspection of the reaction. Figure 4a presents photographs of the aerogel at constant hydrogen flow as the precursor feed rate is reduced from 5 mL/h (less diluted) to 2 mL/h, going from a concentrated aerogel that cannot be substantially drawn (W_{max} = 8 m/min) to a more diluted one that can be spun much faster (W_{max} > 20 m/min) and produce oriented fibers. The dilution of the aerogel can be seen as an increase in its diameter as the feed rate is reduced, which we plot in Figure 4b (details of image analysis in S2). The graph shows a diameter increase of about 20% when reducing the injection rate from 5 mL/h to 2 mL/h. This trend is in line with observations

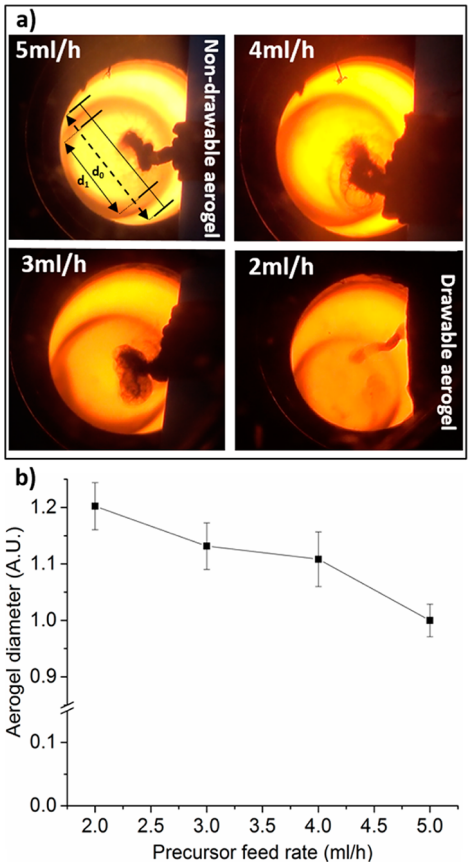

Figure 4. (a) Optical images showing the aerogel expanding as feed rate is decreased. (b) Comparison of aerogel diameter from image analysis showing a 20% increment with dilution.

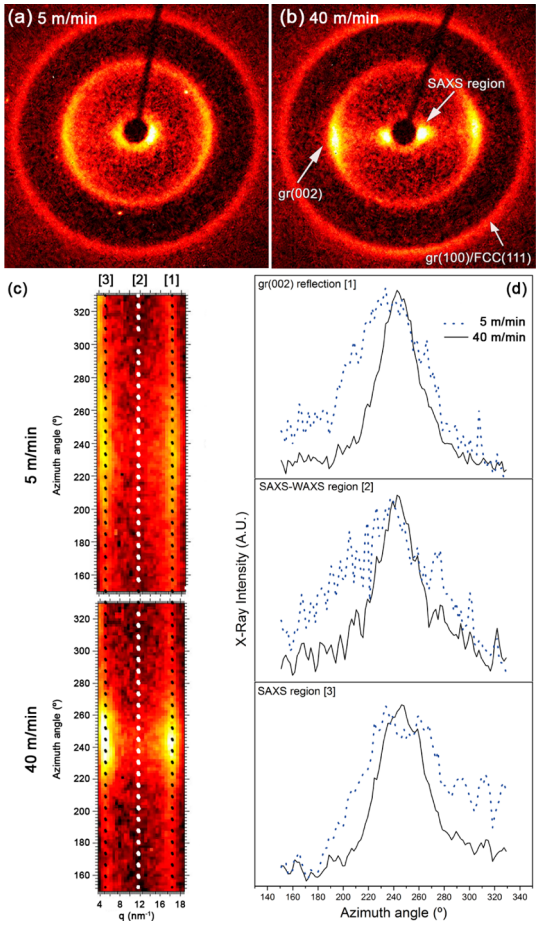

Figure 5. SAXS/WAXS orientation of fibers wound at (a) 5 m/min and (b) 40 m/min. The faster-wound fiber shows (c, d) stronger equatorial (002) reflections from inter- and intra-CNT spacing of basal planes, as well as a sharper SAXS.

of aerogel diameter increasing with higher hydrogen flows in a similar fiber spinning setup.[20] Furthermore, we note that reaction yield in terms of injected carbon/output carbon is not significantly affected by increasing the feed rate and remains around 8.5% (S3).

Entanglements in (Aero)gel Fiber Spinning. The possibility to draw faster a more dilute CNT aerogel occurs because of the reduction in the number of CNT entanglements. This is supported by the fact that although the SWCNT material (0.2 wt % thiophene) has a mass linear density that is about 5 times lower than the MWCNTs (1.5 wt % thiophene), *i.e.*, that the SWCNT aerogel is roughly 5 times less dense than the MWCNT aerogel, both show very similar trends in Figure 2. The implication is that maximum drawing rate does not scale with density of material in the gas phase, but with *number of particles* in the gas phase. Thus, the dilution through adjustment of feed rate or hydrogen flow rates represents a reduction in the number of CNT contact points in the gas phase. The window for drawing then represents conditions under which the aerogel has sufficient CNT association to withstand the frictional stresses associated with dragging it against the gas, but few enough to enable CNT rearrangement during the process.

The mechanism proposed is essentially analogous to polymer fiber spinning and particularly similar to the case of PE. Early work in PE fiber spinning from the melt or cold/hot drawing produced fibers with a tensile strength below 1 GPa and moduli around 70 GPa, significantly lower than those for individual PE crystals. Penning's groundbreaking work produced a large improvement in tensile properties and set the basis of the commercial process for ultrahigh molecular weight PE (UHMWPE) fibers Spectra and Dyneema, by spinning from dilute solutions.[21,22] By lowering the concentration of polymer in paraffin oil, it was possible to produce a gel fiber with reduced number of entanglements, which could then be drawn to higher ratios to produce a higher degree of orientation and crystallinity. As a result, strength as high as 6 GPa and a modulus of 160 GPa were obtained.[23] There are large differences in the persistence length of PE and CNTs (around 10 Å[24] compared to 100 μm[14]), but the comparison of gel and aerogel spinning highlights the common strategy of reducing association of building blocks by lowering their concentration in the (aero)gel state, thus enabling the rearrangement

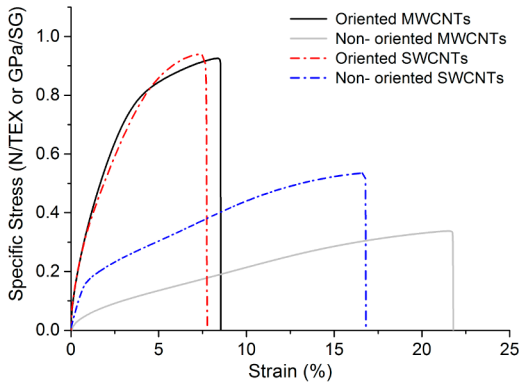

Figure 6. Strain–stress curves for highly and poorly oriented CNT fibers made of SWCNTs or MWCNTs, showing that the degree of orientation dominates over composition in establishing the final mechanical properties of the fiber.

of elements and assembly into a more oriented structure upon drawing.

Orientation and Properties. The expected increase in the degree of orientation upon faster drawing/winding of CNT fibers is confirmed by SAXS/WAXS, as shown in the patterns of Figure 5a and b from fibers produced under dilute conditions and wound at 5 and 40 m/min, respectively. The higher intensity of (002) and SAXS reflections in the equator reflect the alignment of CNTs and bundles parallel to the fiber axis, with the fwhm from azimuthal integration of the (002) decreasing from 76° to 35° (S4). We note that because these samples consist of arrays of >5000 CNT fibers so as to increase X-ray scattering intensity, the orientational distribution might be significantly broadened by fiber misalignment and thus give overestimates of the fwhm compared to individual CNT fiber filaments. The oriented fiber also shows an increased SAXS equatorial component extending to the WAXS region,[25] observable directly in the patterns and in Figure 5c, which shows the azimuthal projection of the patterns in the range $q = 4$ nm^{-1} to $q = 22$ nm^{-1} (from $d = 16$ Å to $d = 2.8$ Å). The packing effect along the SAXS/WAXS region is confirmed by azimuthal integration (Figure 5d), showing a narrow distribution of the X-ray intensity when increasing the winding rate. The emergence of an equatorial SAXS component in the drawn fiber reflects an improvement in packing of bundles at small distances (<2 nm).

Interestingly, mechanical properties are strongly dependent on CNT orientation, to the point that composition in terms of predominant type of CNTs is secondary. Figure 6 presents examples of stress–strain curves of poorly and highly oriented fibers made up of SWCNTs and MWCNTs, respectively. Both oriented fibers have specific tensile strengths around 1 GPa/SG and a modulus close to 40 GPa/SG, compared to 0.3–0.5 and 5–20 GPa/SG for the poorly oriented fibers (histograms in S5 and S6 and table with average values in S7). These results show the importance of

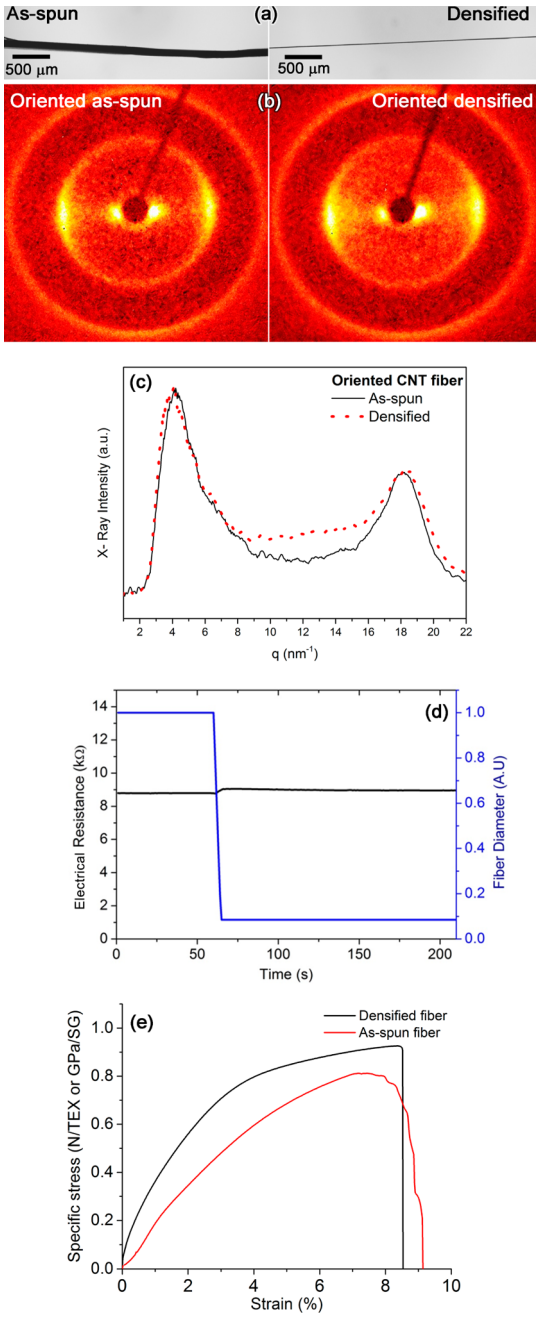

Figure 7. Effects of postspin capillary densification on fiber structure and properties. (a) Optical micrographs of a CNT fiber before and after densification. (b) SAXS/WAXS patterns showing no changes in orientation after postspin densification and (c) equatorial radial profile confirming that CNT and bundle packing at small separations (<2 nm) remain mostly unaltered. (d) Continuous measurement of electrical resistance during the densification process also shows no substantial change in spite of a diameter reduction of an order of magnitude. (e) Stress–strain curves of as-spun and densified fibers with minor differences in strength, modulus, or ductility.

load-bearing elements on a longer length scale than the individual tubes, probably as bundles or fibrils, in determining fiber properties.[26] They also show that the potential of high-performance mechanical properties in CNT fibers is established early in the preassembly

in the gas phase and the orientation imparted by the drawing/winding rate.

Role of Liquid Densification. Finally, we look at the effect of postspin densification (with liquids) on fiber structure properties. This treatment represents a final stage in the process whereby a volatile liquid brought in contact with the CNT fiber exiting the reactor brings its elements together through capillary forces and evaporates before fiber collection, increasing in the process the fiber density by orders of magnitude.[6]

The example in Figure 7a presents optical micrographs of a CNT fiber before and after densification, showing a diameter reduction by a factor of around 11 and therefore a density increase by 120. In spite of such an increase in density, the WAXS/SAXS patterns of these samples (Figure 7b) are nearly identical, with the equatorial radial profile (Figure 7c) showing minor differences. This indicates that neither orientation nor the packing of bundles at small separation (<2 nm) is significantly affected by the densification process. Not surprisingly, postspin densification has a minor effect on fiber properties compared to the pre-established orientation in the gas phase. Figure 7d presents a continuous measurement of electrical resistance during fiber densification. It shows that aside from a transient change upon liquid exposure due to slight swelling,[27] the fiber experiences no net change in resistance and maintains its conductivity per unit mass after a large diameter reduction. Similarly, the comparison of stress−strain curves in Figure 7e shows that fiber modulus and specific strength are not significantly affected by the densification process, at least not comparable with the effect of CNT orientation on fiber properties.

These results demonstrate that postspin densification does not bring elements in the fiber at sufficiently close distances to contribute significantly to charge and load transfer processes. Instead, the network of relevant "points" of interaction in the fiber is fixed earlier in the gas phase during the formation and drawing of the aerogel. Lowering the density of entanglements at the aerogel stage through dilution appears to be a powerful technique to control the assembly of such a network and thus control the final structure properties of the fiber. This possibility will also help clarify the role of CNT composition in terms of number of layers, diameter, and length, which requires comparison of samples with identical degrees of alignment.

CONCLUSIONS

Our results show that in the direct spinning process the association of CNTs in the gas phase is critical in determining the possibility to draw the CNT aerogel and thus produce oriented CNT fibers. The aerogel can be drawn only under dilute conditions, obtained either at a low feed rate of precursors or at a relatively high carrier gas flow rate. These two parameters control the density of CNTs in the gas phase and thus the number of entanglements in the aerogel. Under dilute conditions the aerogel can be drawn as it is pulled against the gas in the reactor (up to 18 draw ratio) and in the process align the CNTs preferentially parallel to each other and to the fiber axis. This requires the aerogel having few entanglements so as to enable the rearrangement of CNTs, yet enough of them to withstand drawing. This situation is similar to wet spinning of high-performance polymer fibers, particularly of polyethylene, where the density of entanglements in solution and the properties of the gel fiber are seen as key stages of the spinning process.

Very importantly, through Raman spectroscopy measurements we show that dilution is achieved without affecting CNT composition, effectively demonstrating the decoupling of synthesis of building blocks from their assembly. Thus, oriented fibers of selected CNTs in the range SWCNT−MWCNT are produced. Their moduli and tensile strength increase upon drawing from around 5 to 40 GPa/SG and from 0.3 to 1 GPa/SG, respectively, with no clear dependence on CNT type observed so far. Accurate evaluation of the role of outer CNT layers in intertube stress transfer, and in general, establishing a quantitative relation between draw ratio, nanotube alignment, and mechanical performance, requires precise measurements of orientation of individual CNT fiber filaments using synchrotron radiation. This will be the subject of a future study.

2D WAXS/SAXS measurements also show that postspin densification, for example through capillary forces upon contact with a volatile liquid, has almost no effect on either the orientation or the packing of CNTs and bundles at small separations. As a result, electrical resistance and tensile properties are largely unaffected by the postspin densification process in spite of a diameter reduction by a factor of 10. These results support the view that the most important CNT assembly in the direct spinning process occurs in the gas phase. The challenge ahead is in controlling CNT association in the aerogel while increasing fiber throughput and without sacrificing control of CNT chemistry and morphology. It will require innovative manipulation methods that can act on the aerogel as it is formed above 1000 °C in a fraction of a second.

METHODS/EXPERIMENTAL SECTION

CNT fibers were synthesized by the direct spinning of CNTs from the gas phase during growth by floating catalyst CVD,[28] using butanol as carbon source, ferrocene as iron catalyst, and thiophene as a sulfur catalyst promoter.[18] The reaction was carried out in a hydrogen atmosphere at 1250 °C, using

different precursor feed rates, carrier gas (H_2) flow rates, and drawing−winding rates.

Scanning electron microscopy (SEM) was carried out with an FIB-FEGSEM Helios NanoLab 600i (FEI) at 5 kV.

Raman spectroscopy was performed using a Jasco NRS-5100, with a laser line of 532 nm corresponding to 2.33 eV. Laser power was fixed at 5.5 mW, and exposure time to 15 s. In order to accurately determine 2D peak positions, all parameters were kept constant to avoid laser-induced peak shifts. Thomas Swan Ltd. Elicarb MWCNTs and SWCNTs were used for comparison.

Small- and wide-angle two-dimensional X-ray scattering patterns were taken at room temperature with a Bruker-AXS SMART 1000 single-crystal diffractometer using Mo Kα radiation and a CCD detector. The sample−detector distance was determined using a silicon single-crystal standard. The X-ray scattering patterns were integrated to obtain radial and azimuthal profiles. The samples used for WAXS/SAXS measurements consisted of multiple parallel CNT fibers produced by winding individual filaments continuously for typically >10 min, corresponding to >1000 filaments.

Mechanical measurements were carried out with a Textechno Favimat using a gauge length of 20 mm. At least 10 samples for each set of synthesis/drawing conditions (*i.e.*, low sulfur−low orientation, low sulfur−high orientation, high sulfur−low orientation, and high sulfur−-high orientation) were tested. Nominal fiber linear density was determined by weighing a known length of fiber (around 30 m). The linear density of samples subjected to tensile tests was further refined using the vibroscopic method.[29] No substantial discrepancies were observed between the two techniques.

Electrical measurements were performed with an Agilent 34410A 6-1/2 digit multimeter using copper tape electrodes and silver paint.

Conflict of Interest: The authors declare no competing financial interest.

Acknowledgment. J.J.V. is grateful to A. Windle for discussions. Financial support from MINECO (Spain), MAD2D project (S2013/MIT-3007, Comunidad de Madrid), and FP7-People-Marie Curie Action-CIG is acknowledged.

Supporting Information Available: Additional sample characterization by Raman spectroscopy (full spectra), details of aerogel diameter determination, calculation of reaction conversion rates, examples of azimuthal profiles of (002) CNT reflection, histograms of tensile strength, modulus, and strain of different fibers. The Supporting Information is available free of charge on the ACS Publications website at DOI: 10.1021/acsnano.5b02408.

REFERENCES AND NOTES

1. Peng, B.; Locascio, M.; Zapol, P.; Li, S.; Mielke, S. L.; Schatz, G. C.; Espinosa, H. D. Measurements of near-Ultimate Strength for Multiwalled Carbon Nanotubes and Irradiation-Induced Crosslinking Improvements. *Nat. Nanotechnol.* **2008**, *3*, 626–631.
2. Dürkop, T.; Getty, S. A.; Cobas, E.; Fuhrer, M. S. Extraordinary Mobility in Semiconducting Carbon Nanotubes. *Nano Lett.* **2004**, *4*, 35–39.
3. Choi, T.-Y.; Poulikakos, D.; Tharian, J.; Sennhauser, U. Measurement of the Thermal Conductivity of Individual Carbon Nanotubes by the Four-Point Three-Ω Method. *Nano Lett.* **2006**, *6*, 1589–1593.
4. Kim, P.; Shi, L.; Majumdar, A.; McEuen, P. L. Thermal Transport Measurements of Individual Multiwalled Nanotubes. *Phys. Rev. Lett.* **2001**, *87*, 215502.
5. Vilatela, J. J.; Eder, D. Nanocarbon Composites and Hybrids in Sustainability: A Review. *ChemSusChem* **2012**, *5*, 456–478.
6. Koziol, K.; Vilatela, J.; Moisala, A.; Motta, M.; Cunniff, P.; Sennett, M.; Windle, A. High-Performance Carbon Nanotube Fiber. *Science* **2007**, *318*, 1892–1895.
7. Liu, Y.; Kumar, S. Polymer/Carbon Nanotube Nano Composite Fibers−A Review. *ACS Appl. Mater. Interfaces* **2014**, *6*, 6069–6087.
8. Behabtu, N.; Green, M.; Pasquali, M. Carbon Nanotube-Based Neat Fibers. *Nano Today* **2008**, *3*, 24–34.
9. Behabtu, N.; Young, C. C.; Tsentalovich, D. E.; Kleinerman, O.; Wang, X.; Ma, A. W. K.; Bengio, E. A.; ter Waarbeek, R. F.; de Jong, J. J.; Hoogerwerf, R. E.; *et al*. Strong, Light, Multifunctional Fibers of Carbon Nanotubes with Ultrahigh Conductivity. *Science* **2013**, *339*, 182–186.
10. Lekawa-Raus, A.; Patmore, J.; Kurzepa, L.; Bulmer, J.; Koziol, K. Electrical Properties of Carbon Nanotube Based Fibers and Their Future Use in Electrical Wiring. *Adv. Funct. Mater.* **2014**, *24*, 3661–3682.
11. Staudinger, H. *Die Hochmolekularen Organischen Verbindungen - Kautschuk und Cellulose*; Springer: Berlin, 1932.
12. Carothers, W. H.; Hill, J. W. Studies of Polymerization and Ring Formation. XV. Artificial Fibers from Synthetic Linear Condensation Superpolymers. *J. Am. Chem. Soc.* **1932**, *54*, 1579–1587.
13. Green, M. J.; Behabtu, N.; Pasquali, M.; Adams, W. W. Nanotubes as Polymers. *Polymer* **2009**, *50*, 4979–4997.
14. Fakhri, N.; Tsyboulski, D. A.; Cognet, L.; Weisman, R. B.; Pasquali, M. Diameter-Dependent Bending Dynamics of Single-Walled Carbon Nanotubes in Liquids. *Proc. Natl. Acad. Sci. U.S.A.* **2009**, *106*, 14219–14223.
15. Vigolo, B.; Pénicaud, A.; Coulon, C.; Sauder, C.; Pailler, R.; Journet, C.; Bernier, P.; Poulin, P. Macroscopic Fibers and Ribbons of Oriented Carbon Nanotubes. *Science* **2000**, *290*, 1331–1334.
16. Ericson, L. M. Macroscopic, Neat, Single-Walled Carbon Nanotube Fibers. *Science* **2004**, *305*, 1447–1450.
17. Lin, L. H.; Edmonds, D. T.; Vollrath, F. Structural Engineering of an Orb-Spider's Web. *Nature* **1995**, *373*, 146–148.
18. Reguero, V.; Alemán, B.; Mas, B.; Vilatela, J. J. Controlling Carbon Nanotube Type in Macroscopic Fibers Synthesized by the Direct Spinning Process. *Chem. Mater.* **2014**, *26*, 3550–3557.
19. Ferrari, A. C.; Meyer, J. C.; Scardaci, V.; Casiraghi, C.; Lazzeri, M.; Mauri, F.; Piscanec, S.; Jiang, D.; Novoselov, K. S.; Roth, S.; *et al*. Raman Spectrum of Graphene and Graphene Layers. *Phys. Rev. Lett.* **2006**, *97*, 187401.
20. Conroy, D.; Moisala, A.; Cardoso, S.; Windle, A.; Davidson, J. Carbon Nanotube Reactor: Ferrocene Decomposition, Iron Particle Growth, Nanotube Aggregation and Scale-Up. *Chem. Eng. Sci.* **2010**, *65*, 2965–2977.
21. Smith, P.; Lemstra, P.; Kalb, B.; Pennings, A. Ultrahigh-Strength Polyethylene Filaments by Solution Spinning and Hot Drawing. *Polym. Bull.* **1979**, *1*.
22. Adams, W. W.; Eby, R. K. High-Performance Polymer Fibers. *MRS Bull.* **1987**, *12*, 22–2.
23. Hoogsteen, W.; Kormelink, H.; Eshuis, G.; ten Brinke, G.; Pennings, A. J. Gel-Spun Polyethylene Fibres: Part 2 Influence of Polymer Concentration and Molecular Weight Distribution on Morphology and Properties. *J. Mater. Sci.* **1988**, *23*, 3467–3474.
24. Flory, P. J. *Statistical Mechanics of Chain Molecules*; Interscience Publishers, 1969.
25. Davies, R. J.; Riekel, C.; Koziol, K. K.; Vilatela, J. J.; Windle, A. H. Structural Studies on Carbon Nanotube Fibres by Synchrotron Radiation Microdiffraction and Microfluorescence. *J. Appl. Crystallogr.* **2009**, *42*, 1122–1128.
26. Vilatela, J. J.; Elliott, J. A.; Windle, A. H. A Model for the Strength of Yarn-like Carbon Nanotube Fibers. *ACS Nano* **2011**, *5*, 1921–1927.
27. Qiu, J.; Terrones, J.; Vilatela, J. J.; Vickers, M. E.; Elliott, J. A.; Windle, A. H. Liquid Infiltration into Carbon Nanotube Fibers: Effect on Structure and Electrical Properties. *ACS Nano* **2013**, *7*, 8412–8422.
28. Li, Y.-L.; Kinloch, I. A.; Windle, A. H. Direct Spinning of Carbon Nanotube Fibers from Chemical Vapor Deposition Synthesis. *Science* **2004**, *304*, 276–278.
29. Gonsalves, V. E. Determination of Denier and Strength of Single Filaments by Vibroscope and Heim Tensile Tester. *Text. Res. J.* **1947**, *17*, 369–375.